Characteristic Morphologies of Conjugated Polymers for Photovoltaic Cells

*This report features the work of Chi-An Dai, Leeyih Wang and their co-workers published in ACS Nano **8**, 1254 (2014), Nanoscale **6**, 2194 (2014), and Macromolecules **47**, 5551 (2014).*

Since polymers were discovered to conduct an electric current, remarkable progress has ensued in synthesizing conjugated polymers, in understanding their properties and in developing their application in photoelectronic devices. Conjugated polymers and their copolymers are regarded as most promising materials for new photovoltaic devices because of their excellent thermal and chemical stability, decreased costs and their tunable electronic and optical properties. Poly(3-hexylthiophene) (P3HT) has rapidly gained attention for use in organic solar cells, light-emitting diodes and thin-film transistors. The photoelectric properties of the fabricated devices are generally accepted to depend critically on the nanostructural forms of P3HT. To understand the kinetics of polymer crystallization and its correlation with morphological developments of conjugated polymers would hence provide notions about the optimal processing of future photovoltaic devices. Small-angle X-ray scattering (SAXS) and X-ray diffraction at TLS end stations BL23A and BL13A respectively captures the kinetics of conjugated polymer crystallization in the corresponding photovoltaic devices.

A research team comprising Chi-An Dai and Leeyih Wang at National Taiwan University and their associates has identified critical structural characteristics, polymorphic crystals and phase transformations in P3HT-based polymers, including nanohybrid,[1] rod-coil block copolymer[2] and rod-rod block copolymer,[3] for solid-state dye-sensitized solar cells or photovoltaic devices. In the case of a P3HT/zinc oxide (ZnO) hybrid,[1] they proposed a synthetic method to fabricate *in situ* self-assembled organic and inorganic hybrid nanowires. This facile method can simultaneously organize P3HT chains and inorganic zinc precursors into highly ordered nanowires with length on a μm scale, followed by thermal oxidation to grow discrete ZnO nanocrystals directly on the existing P3HT nanowire template. After thermal annealing, the reorganization of the crystal structure of P3HT to yield chain axes highly oriented perpendicular to the fibril axis results in the segregation of ZnO nanocrystals into the surface of the crystalline P3HT nanowires to form a unique donor-acceptor parallel-lane nanowire network structure composed of alternating coextensive lanes of ZnO nanocrystals and P3HT nanowires that form the electron-acceptor channels (Figs. 1(a) and 1(c)). In Fig.

1(b), a grazing-incidence wide-angle scattering (GIWAXS) pattern exhibits intense arcs associated with the $(100)_{P3HT}$, $(200)_{P3HT}$ and $(300)_{P3HT}$ reflections along the q_z axis (substrate normal) and the $(020)_{P3HT}$ reflection along the q_{xy} axis (substrate parallel), indicating that the π-conjugated planes of P3HT block are parallel with respect to the substrate. Three diffraction maxima in higher q_{xy} were assigned to planes (100), (002), and (101) corresponding to the wurtzite structure of ZnO, confirming the presence of crystalline nanoparticles. On measuring the photovoltaic efficiency of P3HT/ZnO hybrid devices, they found that the donor-acceptor parallel-channel structure gave access to improved dissociation of excitons and charge transport, thereby enhancing quenching of photoluminescence, charge transport and device performance. The photovoltaic devices with a donor-acceptor parallel-lane structure of P3HT/ZnO hybrid gave PCE 0.61% relative to only 0.07% from a conventional P3HT/ZnO bulk heterojunction solar cell.

On investigation of poly(3-hexyl thiophene)-*b*-poly(2-vinyl pyridine) P3HT-*b*-P2VP,[2] they reported a new approach to control the polymorphs and nanostructures of the copolymer for future applications using processing in solution and subsequent thermal treatment. Figures 2(a)-2(b) show the temperature-dependent profiles of SAXS and wide-angle X-ray scattering (WAXS) from *in situ* measured during a step-wise heating course. In the WAXS profiles (Fig. 2(b)), observed diffraction maxima at $(100)_{II}$, $(200)_{II}$ and $(020)_{II}$ below 80 °C indicated the self-assembly in solution of P3HT-*b*-P2VP first formed from II crystals of P3HT within its nanofibrillar core confined by P2VP blocks in the surrounding domain. Distinct from a mixture of form-I and form-II crystals in a P3HT homopolymer, the formation of the rare form-II crystals is attributed mainly to the consequence of a slow crystallization of the P3HT block under the nanoconfinement imparted by neighboring P2VP blocks along the crystal growth during drying. With increasing temperature and then cooling, a new phase transformation from form-II crystals to form-I crystals is observed in Fig. 2(b). Upon heating the sample further

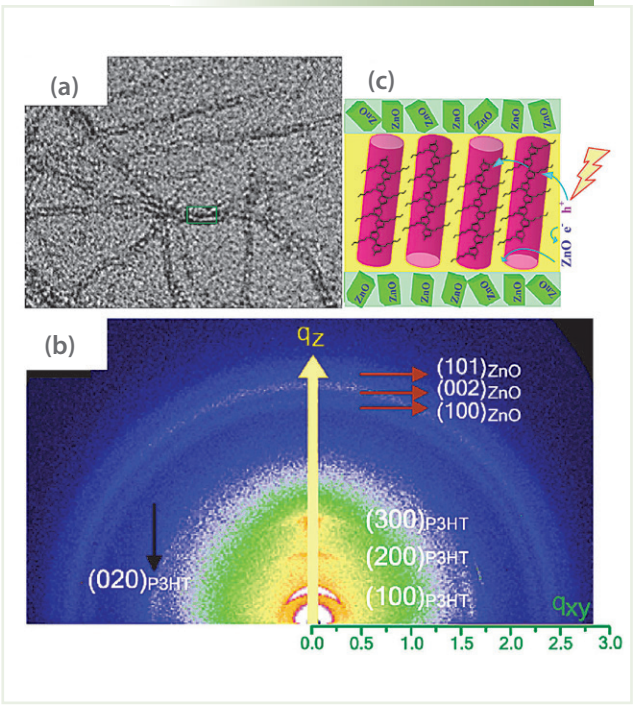

Fig. 1: (a-b) TEM micrograph and GIWAXS pattern of P3HT/ZnO hybrid. (c) Cartoon for a donor-acceptor parallel-lane nanowire structure. PTh_4BT and PTh_4FBT before and after thermal annealing. (Reproduced from Ref. 1)

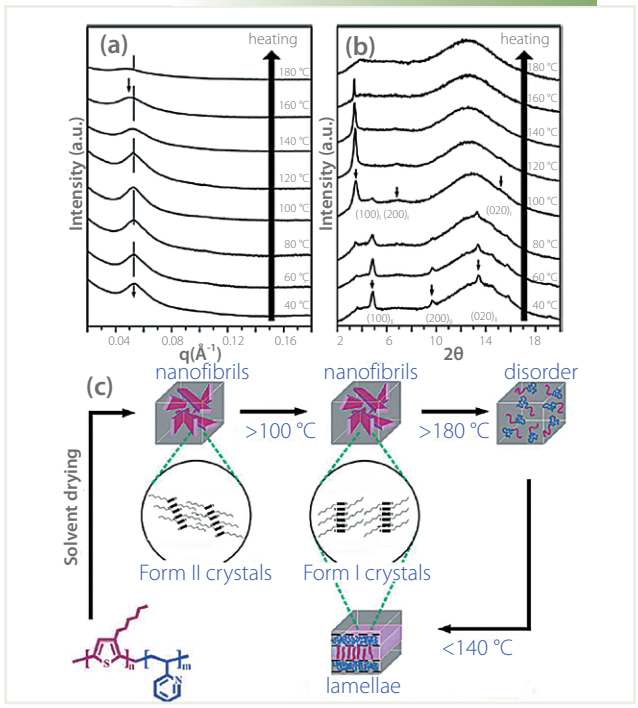

Fig. 2: (a, b) SAXS and WAXS profiles for the solvent-cast sample of P3HT-*b*-P2VP on step-wise heating; (c) Cartoon for the route of phase transformations of solution-dried P3HT-*b*-P2VP. (Reproduced from Ref. 2)

to 120 °C, new sharp and intense diffraction signals associated with planes $(100)_I$ and $(020)_I$ emerge, showing the phase transformation from form-II crystals to form-I crystals. At temperature 160 °C, the WAXS profiles correspond to weak (100) diffraction, indicating a nematic liquid-crystalline structure of P3HT. Figure 2(c) illustrates schematically the structural evolution and phase transformation including the mesoorder–disorder, order–order and polymorphism transitions from a solvent-cast sample of P3HT-*b*-P2VP.

These workers synthesized poly(2,5-dihexyloxy-*p*-phenylene)-*b*-poly(3-hexylthiophene) (PPP-*b*-P3HT) and applied it as a material for hole transport (HTM) in dye-sensitized solar cells.[3] WAXS profiles in Fig. 3 show diffraction signals for PPP-*b*-P3HT block copolymer and two homopolymers of PPP and P3HT. The PPP-*b*-P3HT exhibits diffraction signals (100), (200) and (300) similar to those obtained from the crystalline P3HT homopolymer, whereas no diffraction signal in the WAXS profile was associated with PPP for the copolymer. These observations clearly verify that the P3HT segments in the block copolymer tend to form a crystalline supramolecular structure through π-π stacking of the P3HT during the spin drying, but the PPP block remains an amorphous structure. From measurements of transient photovoltage, they found that the photovoltaic cell based on PPP-*b*-P3HT as a HTM has a greater electron lifetime than that of the reference device based on P3HT homopolymer. These findings indicated that amorphous PPP segments in the copolymer improve the molecular packing of the P3HT blocks to form interpenetrating fibrils with long-range order during spin drying, leading to a hole mobility for the block copolymer greater than that of the parent P3HT homopolymer with a comparable molar mass. Moreover, the PPP chain significantly improves both the completeness and tightness of the HTM coverage on top of the sensitized titania such that the probability of carrier recombination is decreased, yielding a significant advance in photovoltaic performance.

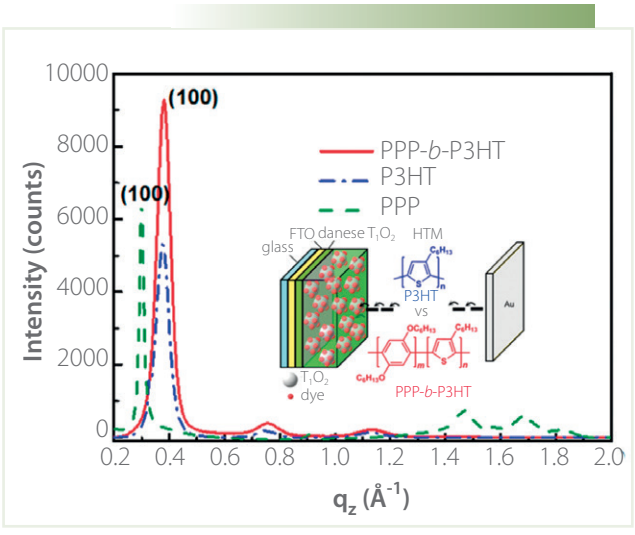

Fig. 3: WAXS profiles of PPP-*b*-P3HT, P3HT and PPP films. (Reproduced from Ref. 3)

In summary, their new findings a detailed understanding of the dependence of self-assembly of P3HT based polymers on both kinetic and thermodynamic effects and offer guidance for the morphological control and optoelectronic properties in the device applications. (Reported by Wei-Tsung Chuang)

References

1. Y. H. Lee, Y. P. Lee, C. J. Chiang, C. Shen, Y. H. Chen, L. Wang, and C. A. Dai, Macromolecules **47**, 5551 (2014).
2. Y. H. Lee, Y. L. Yang, W. C. Yen, W. F. Su, and C. A. Dai, Nanoscale **6**, 2194 (2014).
3. W. C. Chen, Y. H. Lee, C. Y. Chen, K. C. Kau, L. Y. Lin, C. A. Dai, C. G. Wu, K. C. Ho, J. K. Wang, and L. Wang, ACS Nano **8**, 1254 (2014).